

Miniaturized Wideband MIMO Antenna based on Hybrid Isolation Technique

Ahmed Read Al-Tameemi, Goh Chin Hock, Tiong Sieh Kiong, Taha Raad Al-Shaikhli, Mohammed S. Al Ani, and Mohammad A. K. Al Ani

Abstract—A compact wideband two-port multi-input-multi-output (MIMO) antenna for 5G sub-6 communication is proposed in this research. The MIMO antenna consists of a coplanar waveguide and a Moore fractal based on the second iteration, comprising two T-stub shapes designed to achieve the desired frequency band and enhance the capacitive coupling effect. To improve the return loss and isolation between the two elements, closed rectangular ring metamaterials and a neutralization line are incorporated, resonating across 2.7–5.3 GHz (2.55 GHz) with high isolation below -20 dB for the entire frequency band. The proposed antenna has dimensions of $31 \times 50 \text{ mm}^2$ with thickness of 1.6mm. The suggested MIMO design is fabricated using low-cost FR4, and its S-parameters, gain, and radiation patterns are measured. Simulation and fabrication measurements demonstrate an envelope correlation coefficient below 0.005, indicating excellent spatial diversity performance. Additionally, the capacity loss is found to be less than 0.3 b/s/Hz, highlighting the antenna's efficiency in maximizing data transmission rates for 5G sub-6 communication.

Index terms—Antenna, MIMO, isolation techniques, wideband, energy.

I. INTRODUCTION

The technology of MIMO has been extensively employed in many systems to increase channel capacity [1]. The growth of mobile communication has been driven by the rising demand for wireless traffic. The three primary advancement trends in mobile communication systems are broadband, high transmission data rates, mobility, and intelligence. Current-generation (5G) mobile communication systems must support more diverse scenarios and address significant performance challenges compared to previous-generation (4G) systems [2].

Recently, the demand for compact MIMO antennas for 5G sub-6 communication with high capacity has increased.

Manuscript received October 9, 2024; revised December 16, 2024. Date of publication March 25, 2025. Date of current version March 25, 2025. The associate editor prof. Zoran Blažević has been coordinating the review of this manuscript and approved it for publication.

A. R. Al-tameemi, G. C. Hock, T. S. Kiong are with the College of Engineering, Universiti Tenaga Nasional, Kajang, Malaysia (e-mails: ahmed.itm@nuc.edu.iq, {chinchock, SiehKiong}@uniten.edu.my).

T. R. Al-Shaikhli is with the Department of Computer Engineering, University of Technology, Baghdad, Iraq (email: taha.r.eng@uotechnology.edu.iq).

M. S. Al Ani is with the College of Engineering Technology, Al-Farahidi University, Baghdad, Iraq (mr.muhammed.salim@uofarahidi.edu.iq).

M. A. K. Al Ani is with the Department of Computer Engineering Al-Nisour University College Baghdad, Iraq (email: mohammed.itm@nuc.edu.iq).

Digital Object Identifier (DOI): 10.24138/jcomss-2024-0077

However, designing compact MIMO antennas requires researchers to place the antenna elements close to each other, which introduces new design challenges. In return, antenna performance in term of isolation, frequency band, bandwidth, radiation, gain will be deteriorated. Therefore, many researches developed a different technique to solve this issue and decrease the coupling depend on antenna structure.

MIMO (Multiple-Input-Multiple-Output) technology has attracted considerable interest in recent years because of its potential to improve data rates, capacity, and spectral efficiency in modern wireless communication systems, including 4G, 5G, and beyond. To enhance the performance of MIMO antennas, many designs have been developed that focus on mitigating mutual coupling, a key issue that can negatively impact system performance if left unaddressed. In [3], two port MIMO antenna based on custom fractal with coplanar waveguide proposed for 5G sub-6. The port positioned on the front view of substrate with separating space of 6mm. The result shows a strong coupling between closed elements. Therefore, t-reflected stub placed between antenna elements to enhance the isolation below -10dB. A two-port MIMO antenna based on a T-stub CPW with a Hilbert fractal is proposed in [4]. An EBG structure is placed on the bottom surface of the plane to enhance the isolation to below -20 dB. A wideband two-port MIMO antenna is presented in [5].

Referring to [6], two elements located on top of substrate with distance about 11mm. To enhance the isolation, a two inverted L shaped stripe loaded among the antenna elements to be below -15dB. In addition, there is different techniques used to improve the isolation like defect ground structure DGS which is used in [6].

In this work [6], two square microstrip line was printed in the front view of substrate as a radiator element for sub-6 5G. To enhance the isolation from -12dB to -20dB, a modified rectangular shape etched on partial ground plane. In [7] T-shaped ground plane used to reduce the coupling below -26dB at the worst situation. In [8], a taper feed with full rhombic ring presented and modified to operate at quad frequency band. The partial ground plane also modified to improve isolation below -13dB as a minimum isolation and below -34dB as maximum isolation. In addition, a neutralization line (NL) was used in [10] to improve the isolation between the eight F-shaped monopole elements to below -16 dB. In [11], an NL was printed between circular monopole antennas to reduce the isolation to less than -15 dB. However, in this study [12], a self-isolation

technique was used to enhance the isolation, depending on the distance between the antenna elements and their orientation. The presented antenna achieved an ultra-wideband with a minimum isolation of -18 dB.

Additionally, the literature has focused on the metamaterial (MTM) technique [14]–[16]. In [14], two layers of the substrate were used, with the bottom layer acting as a reflector and the upper layer acting as a radiator of two orthogonal double-loop dipoles, designed to operate at dual bands with maximum coupling less than -15 dB and better isolation below -25 dB. Nevertheless, in [15], an EBG MTM structure was inserted between the two radiator elements to achieve coupling less than -20 dB for all operating bands. Finally, a parasitic element of a T-stub ground branch was used in [17] to improve the isolation between two monopole radiating elements. The presented study achieved isolation below -20 dB and below -45 dB at 3.4 GHz.

The proposed antenna design process, which utilizes a hybrid technique combining MTM and NL techniques, represents a significant advancement over the authors' previous works. This hybrid approach is specifically aimed at improving the performance of MIMO antennas, addressing key challenges such as mutual coupling, bandwidth enhancement, and radiation efficiency. While the related work section discusses similar methodologies and foundational principles, this paper introduces a novel integration of MTM and NL techniques.

In this paper, a high-isolation, two-element MIMO antenna is proposed and analyzed, operating within the 2.76 to 5.32 GHz range, making it suitable for the sub-6 GHz 5G frequency band. The antenna elements consist of two T-stub coplanar waveguides surrounded by a Moore fractal based on the second iteration, placed with a small spacing of 7.1 mm to achieve a compact MIMO antenna design. Four closed rectangular ring metamaterial (CRR) structures are inserted between the antenna elements to suppress the propagation of surface waves. Additionally, a neutralization line technique is employed on the bottom surface of the plane to further enhance decoupling. As a result of these design optimizations, the isolation between the antenna elements is improved to below -20 dB across the entire operating frequency range.

The main contributions of this study are as follows:

- Various isolation techniques have been studied and applied in previous works to enhance isolation. However, in this study, two isolation techniques are employed to improve two key properties: isolation and impedance matching. This is achieved through the use of closed rectangular ring metamaterials and a neutralization line. The proposed design exhibits wideband behavior from 2.76 GHz to 5.32 GHz, with a maximum coupling of less than -20 dB.
- The compact size of the MIMO antenna is maintained, with a spacing of 7.1 mm between the antenna elements and an overall size of $31 \times 50 \times 1.6 \text{ mm}^3$.

This paper is structured as follows: Section III outlines the research method, design procedures, and working mechanism. Section IV presents and discusses the measured results of the fabricated antenna. Section V presents a comparison with related works. Finally, Section VI provides a brief summary of the conclusions

II. RESEARCH METHOD

The proposed design of the suggested MIMO antenna is illustrated in Figure 1 below. The feed structure utilizes a coplanar waveguide (CPW), Moore fractal, T-stub, and three square-shaped metamaterials (MTM). These geometries are printed on the same FR4 substrate, which has a relative permittivity of 4.7 and a loss tangent ($\tan \delta$) of 0.025. The proposed geometry is arranged as a two-port MIMO antenna. The overall dimensions of the antenna are $50 \times 31 \text{ mm}^2$ with a thickness of 1.6 mm. The use of CPW in this geometry is advantageous because the transmission line and ground plane are positioned on the same surface of the substrate. As a result, the patch operation experiences minimal interference from surface waves generated in such a structure [18]. Additionally, the small spacing between the ground plane and the T-stub plays an effective role in controlling and improving the bandwidth of the proposed structure by maximizing or minimizing the air gap [19]. Furthermore, the various fractal paths contribute to the antenna's multi-frequency resonance behavior. The study suggested to use the second iteration of Moore fractal surrounded the T-stub fed line and generate a capacitive coupling in the gap between them [20]. As result, the isolation between the t-stub and fractal geometry. to realize multiple band behaviour, an electric field need to connect to surround with Moore fractal. Due to the impact of conservation losses in the resultant capacitor, significant losses may be realized during such a process. To eliminate the impacts of the capacitive load, it is crucial to take this into account when building the patch shape. Additionally, it is crucial to consider the impacts of the capacitive load in order to increase the antenna bandwidth for the suggested applications [19], [20]. Therefore, using the suggested MTM structure's layered boxes satisfies the requirement for the number of bands formed Such an MTM is intended to be done away with coupling's effects in the targeted frequency range.

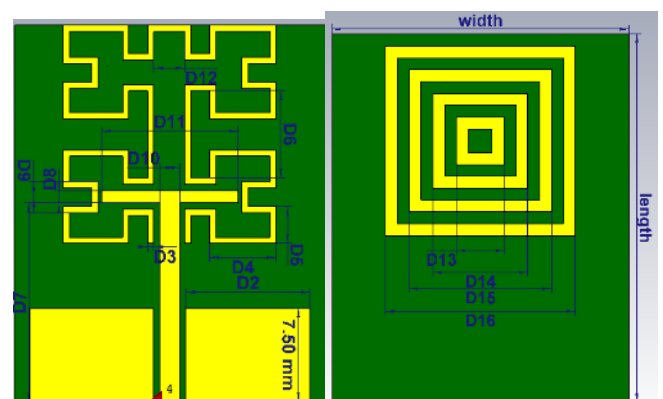


Fig.1. The front and back view dimensions of the antenna design text.

A. Single patch study

To obtain the appropriate bands, the design dimensions were gradually optimized for 5G communication's lower frequency. To calculate the antenna dimensions this study used the equation below [29]:

$$w = \frac{c}{f_r \sqrt{\frac{\epsilon_r + 1}{2}}} \quad (1)$$

where w is representing width of patch, f_r is the frequency resonant (3.5 GHz), ϵ_r is relative permittivity (4.7), c is defined as a speed of light in empty space. effective dielectric constant is calculated via:

$$\epsilon_{reff} = \frac{\epsilon_r + 1}{2} + \frac{\epsilon_r - 1}{2} \left(1 + 12 \frac{h}{w}\right)^{-1} \quad (2)$$

The units of h and w present length and width of patch. where effective length L_{eff} need to be calculated via:

$$L_{eff} = \frac{c}{2f_r \sqrt{\epsilon_{reff}}} \quad (3)$$

The fringing length (ΔL) is calculated by equation:

$$\Delta L = 0.412 \frac{(\epsilon_{reff} + 0.3) \left(\frac{w}{h} + 0.264\right)}{(\epsilon_{reff} - 0.258) \left(\frac{w}{h} + 0.8\right)} \quad (4)$$

The length (L) of proposed antenna patch is calculated via

$$L = L_{eff} - 2\Delta L \quad (5)$$

Figure 1 demonstrates the proposed antenna geometry and the dimensions of each element also listed in Table 1. In this study, the antenna geometry printed on low cost FR4 with dielectric constant of $\epsilon_r = 4.7$, $\tan \delta = 0.025$ with dimension of $31 \times 25 \times 1.6 \text{ mm}^3$. The section below explains the improvement steps of the antenna.

TABLE I
THE PROPOSED ANTENNA'S DIMENSIONS

parameters	Dimension (mm)	Parameters	Dimension (mm)
Width	25	length	31
D1	7.5	D9	2.5
D2	10	D10	2
D3	0.5	D11	11
D4	5.27	D12	3.5
D5	2.97	D13	4
D6	8.04	D14	8
D7	16	D15	12
D8	1	D16	16

A.1 T-stub

In this study, the authors used T-stub to sustain the reduction in antenna size and to guarantee a high field gradient. So, parametric study is applied on T-stub to improve the antenna properties. then, it's started by changing the width of T-stub from 7 to 11 mm with step of 1mm and investigate the effect of S_{11} . The presented result in Figure 2 shows a reveals negligible fluctuation in the resonance frequency caused by altering the parameter width. However, when the width of T-stub maximizing the return loss of operating frequency also increasing as well. So, the authors found that the T-stub (width = 7) is the best option, since it has best return loss at the frequency resonant.

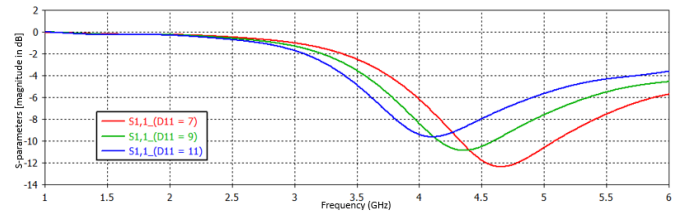


Fig. 2. S11 parameter of the antenna with different widths of T-stub.

A.2 Moore fractal

In this step, a parametric study was conducted to determine the optimal Moore fractal iteration for the proposed design. The study began by loading the 1st, 2nd, and 3rd iterations of the Moore fractal onto the T-stub CPW patch and observing how these changes affected the S-parameters of the antenna. As shown in Figure 3, the frequency resonance of the antenna increases as the number of Moore fractal iterations increases. This behavior can be attributed to the enhanced effective electrical size of the antenna, achieved by extending the antenna's surface current path, which improves space usage and space-filling performance [19]–[21].

However, this study selected the 2nd iteration due to its significant effect on antenna performance. The red curve in the figure indicates an improvement in impedance matching for both the first and second frequencies. Additionally, the second frequency band shifts closer to 3.5 GHz with a return loss below -22 dB.

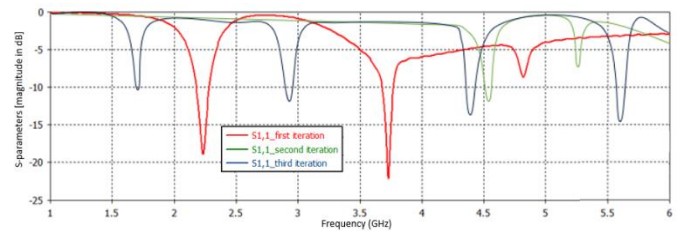


Fig. 3. S-parameter of changing the iterations of Moore fractal.

A.3 Closed square rings (CSRs)

To further enhance the performance of the proposed antenna, four Closed Square Ring (CSR) resonators were added to the bottom surface of the design to improve the return loss, bandwidth, and gain. The closed square ring resonator creates a resonant circuit that is straightforward, affordable, and easy to fabricate using a common photolithographic process. When the cavity resonates, and the round-trip phase shift of the waves in the four square loops equals an integer multiple of 2π , a positive interaction between the waves occurs [22]. As shown in Figure 4, all the frequency bands shift, resulting in an improved return loss and bandwidth. The first frequency band starts resonating at 3.3 GHz with an enhanced bandwidth of approximately 0.53 GHz. Additionally, the second frequency band shifts to resonate at 5.3 GHz with an improved bandwidth of about 0.3 GHz. Moreover, the effects of printing the four CSRs on the back view of the antenna were analyzed with respect to the gain curve. As seen in Figure 4(b), there is a significant improvement in the radiation properties of the antenna.

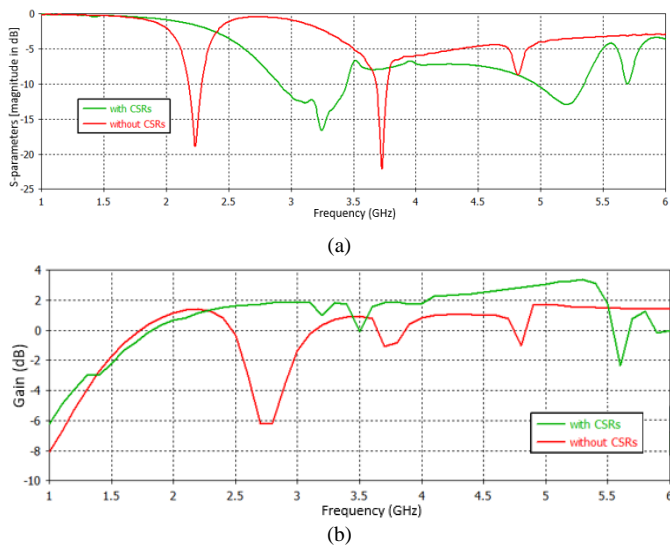


Fig. 4. Antenna performance: a) S-parameter, b) gain.

A.4 Coplanar waveguide effects

In the proposed geometry, the authors utilized CPW with a T-stub to feed the antenna. To validate the effects of varying the gap between these components, a numerical study was conducted by altering the gap width from 0.3 mm to 1.2 mm while monitoring the effects on S_{11} . As shown in Figure 5(a), it was observed that increasing the gap width improved the return loss of the second frequency resonance. However, at the same time, the first frequency band was negatively impacted, losing its return loss. This behavior is attributed to the increased capacitive coupling loss in relation to the T-stub, which amplifies the surface current in the air gap [18]. The study concluded that maintaining a minimal gap of 0.3 mm is the optimal choice for performance.

Additionally, to further enhance the return loss of the proposed geometry, another parametric study was conducted on the width of the T-stub after integrating all the above structures. The study involved varying the width from 3.5 mm to 5.5 mm in increments of 0.5 mm and observing its impact on the S-parameters. As depicted in Figure 5(b), minimizing the gap between the T-stub and the fractal geometry maximized the return loss. It was found that when the width was set to 5.5 mm, the antenna operated at dual bands of 3.5 GHz and 5.3 GHz with return losses below -19 dB and -15 dB, respectively, and a slight improvement in bandwidth.

This improvement can be explained by the surface-wave diffraction and the influence of the Moore geometry's enhanced inductive coupling. The strong capacitive coupling generated when the T-stub's edge and the Moore body are in close proximity increases the electromagnetic field interaction with the Moore body [4]. Consequently, the study considered a width of 11 mm for the design.

B. MIMO antenna study

In this section, we will discuss the mechanism creation of MIMO array based on proposed geometry and the steps of characteristic MIMO enhancements.

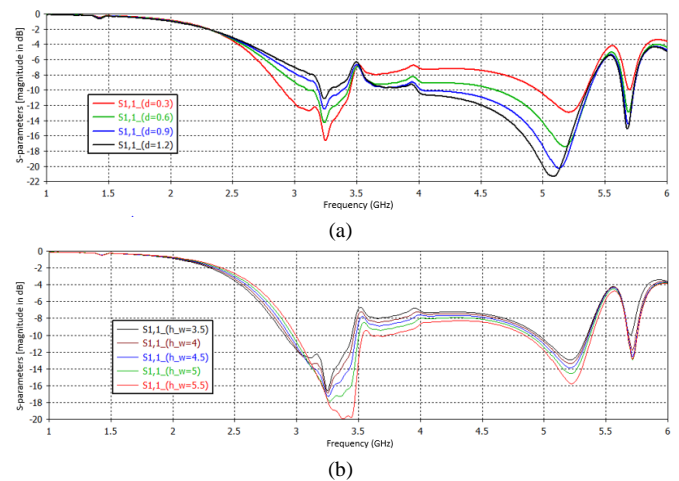


Fig. 5. S-parameter of changing the width of: (a) gap between T-stub and ground plan (b) change the width of T-stub.

B. 1 Without isolation technique

In this step, the geometry and structure of the proposed 2-port MIMO antenna are illustrated in Figure 6, which is created by two single-element antennas were designed in the section above. The two port MIMO are arranged in a horizontally pattern at the same substrate. The minimum inter-element spacing between the MIMO antenna elements is 7.1 mm to keep the size of MIMO as compact. The whole size of this modification is $50 \times 31 \text{ mm}^2$ as shown in figure 6 (a). The effects of the creation this structure on the S-parameters is illustrated in figure 6 (b). The blue curve describes the creation MIMO antenna has dual band resonance at 2.8 and 5.2 GHz with bandwidth of 0.95 and 0.3 GHz respectively. However, the orange curve explains the coupling between the two adjacent elements was strong below -6 dB at 2.8 GHz due to the small distance between the antenna elements while one of ports excited, the electromagnetic field will transfer to the close ports and therefore the coupling became strong. So, to enhance the isolation between the antenna, authors investigated many types of modification on the proposed structure and found that the best option was by remove the two middle two squares of CPW between the two elements. In figure 6 (b) below shows the green curve illustrates the coupling after this modification. As seen, the isolation improved from -6 dB to -10 dB at the same frequency resonance (2.8 and 5.2 GHz).

B. 2 With CRRs MTM

In this section, three closed rectangular rings CRRs as shown in figure 7 (a) will be inserted between the T-stub. This MTM structure dimensions has calculated to be places among two elements to increase the isolation and enhance the matching impedance across the desired bandwidth. Figure 7 (b) depicts simulated S-parameters with and without inserted CRRs MTM between the elements. The figure 7 (b) shows that antenna have a wideband behavior from 2.76 to 5.32 GHz with minimum coupling of -13dB after insert CSRs MTM. A matching circuit made of capacitances (the distance through the ring stripes) and inductances (the width of the ring-shaped stripes) could used to describe the changes in S-parameters [23]. Also, the result shows there is an enhancement of isolation at the desired

frequencies from -15dB to -19dB at 3.5 GHz and from -22dB to -32dB at 5.2GHz. Therefore, the proposed CRRs MTM has significant impact on the MIMO antenna performance.

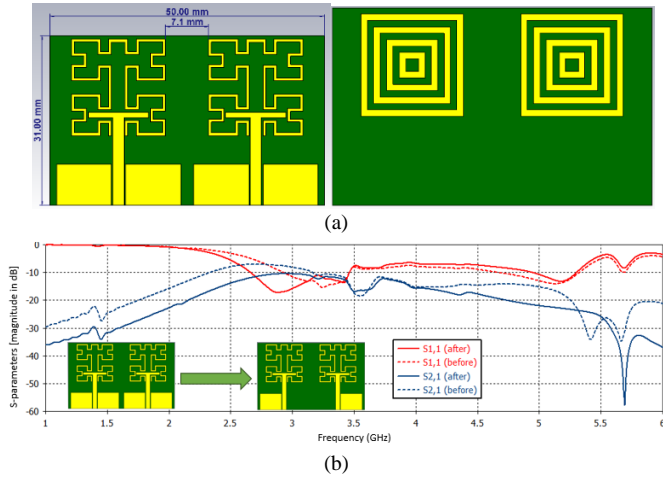


Fig. 6. MIMO Antenna: a) geometry, b) S-parameter.

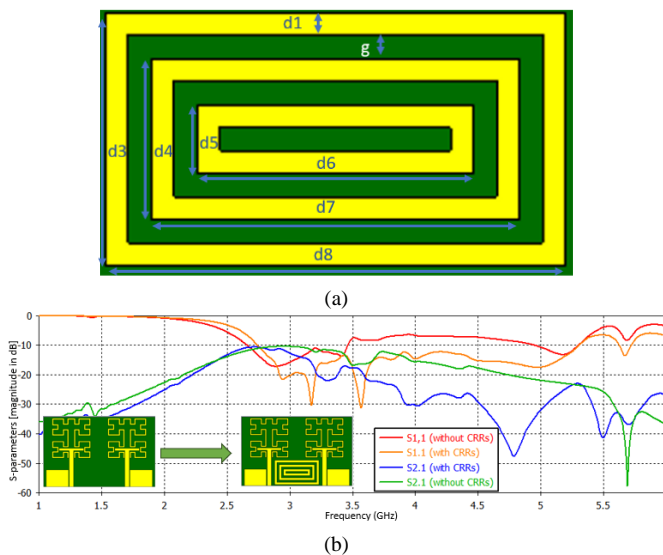


Fig. 7. MIMO Antenna: a) CRRs dimensions: $d1=1\text{mm}$, $g=1\text{mm}$, $d3=11\text{mm}$, $d4=7\text{mm}$, $d5=3\text{mm}$, $d6=12\text{mm}$, $d7=16\text{mm}$, $d8=20\text{mm}$, b) S-parameter before and after load CRRs MTM.

TABLE II
THE PROPOSED ANTENNA'S DIMENSIONS

parameters	Dimension (mm)	Parameters	Dimension (mm)
d1	1	g	1
d3	11	d4	7
d5	3	d6	12
d7	16	d8	20

B. 3 With neutralization line NL

In the previous step, the mechanism for improving the isolation between the two elements led to good results. However, still needs to reduce the coupling at frequency bandwidth from 2.7 to 3.3 GHz. The core concept of this approach was to counteract the intricate electromagnetic coupling between adjacent antennas by using an opposing

coupling reaction. Since the coupling between the antennas is capacitive, the line primarily serves to generate an inductive response that counterbalances the capacitive effect of the antenna coupling. Therefore, the study loaded a NL at the back view of substrate with conduct an analysis of the parametric research on the width of NL and surface current to thoroughly evaluate the impact of the NL added between elements.

The parametric study applied on width of NL and started from 0.4mm to 2mm with step of 0.8mm as shown in figure 8 below the effect S_{12} while the value is changing. As seen, when the width of NL maximize, the isolation at the operating frequency band is improved to be below -21dB when the value of NL width equal 2mm. It's happened because of the termination the electromagnetic surface wave to be transformed to close element when the post excited.

Figures 8(b) shows the surface current distribution when first Port has been connected to an excitation source and the second port is matched to a -50dB load. When the NL is placed in the middle of these two components, as shown in Figure 8(b), its clearly that NL act as a surface current preventer to into Port 2. Therefore, its obvious that the current density at Port 2 is lower than the surface distribution of without NL[24].

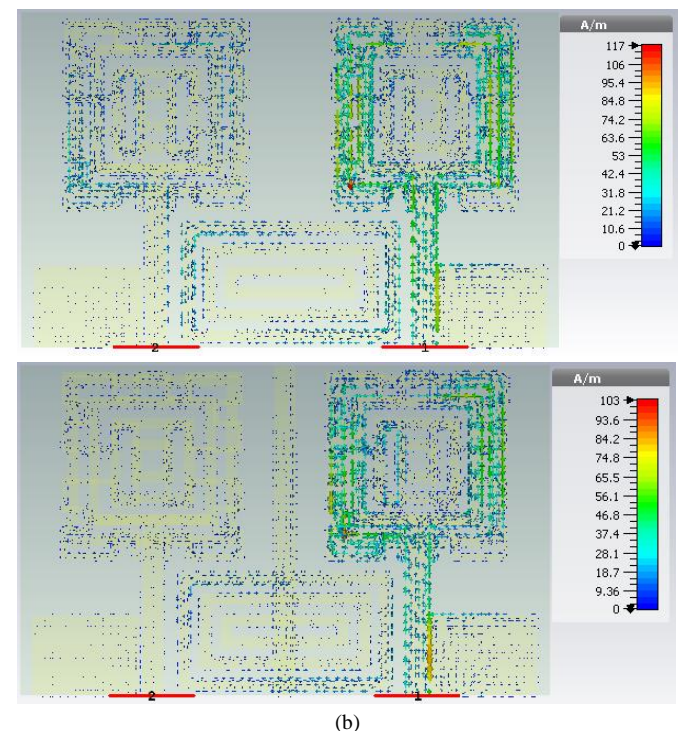
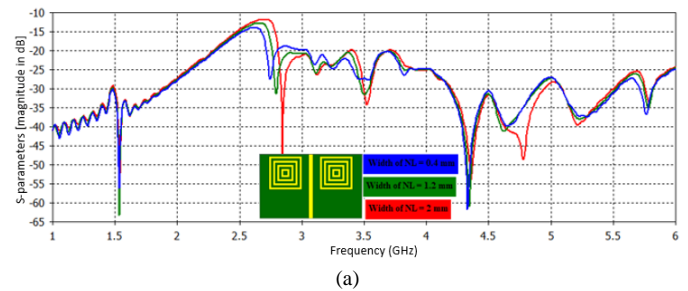


Fig. 8. Antenna performance: a) effect of change the width of loaded NL on S_{21} , b) Surface current before and after load NL.

III. RESULTS AND DISCUSSION

A simulation and parameterization process were used to maximize the proposed antenna's parameters by using CST software. After that, the enhanced model was built in order to evaluate its measured performance. Figure 10 shows a picture of a constructed MIMO antenna.

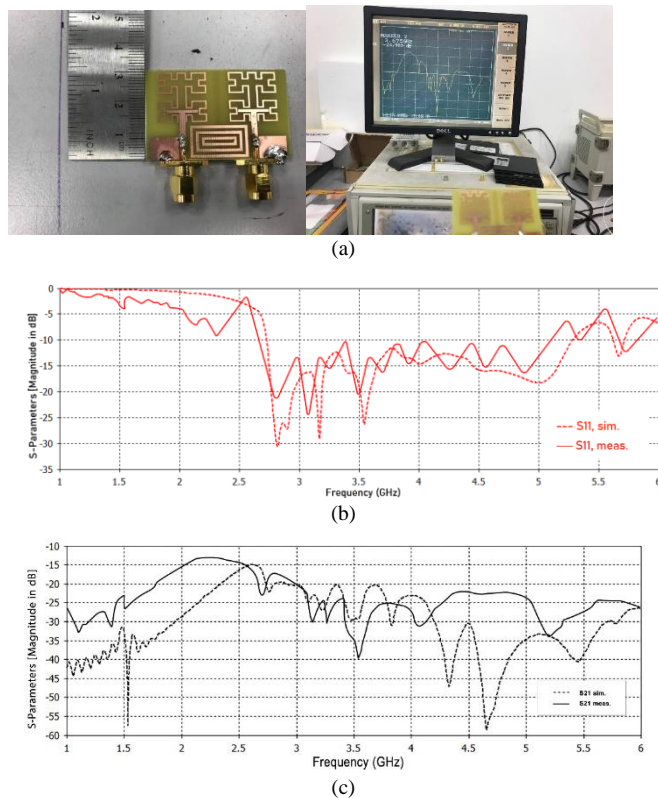


Fig. 10. Assessment of the antenna array's performance involves examining (a) the manufactured prototype and transmission coefficient, (b) S11, and (c) S12.

A. Reflection and transmission coefficients

To investigate the S-parameters of the fabricated design, the VNA used for this purpose. In Figure 10, the plotted measured and simulated S-parameters of the proposed design are compared, revealing a strong agreement between them. The reflection coefficient of port (1) and port (2) must be below -10dB and the transmission coefficient of two ports must be below -20dB demonstrate satisfactory impedance matching and enhanced reduction of mutual coupling across the entire wide band (2.7 GHz to 5.1 GHz). An outstanding isolation, registering below -27dB at the required frequency was achieved. Any minor discrepancies observed between the measured and simulated results can be attributed to manufacturing and connection tolerances during the fabrication process.

B. Radiation pattern

Following fabrication of the MIMO antenna design underwent testing in an Anechoic chamber to assess its radiation characteristics across various frequencies. The measurement and calculation of radiation patterns are

illustrated in Figure 11, displaying both azimuth (left) and elevation (right) planes at frequencies of 3.5GHz and 5GHz.

The radiation pattern experimental results were derived by energizing first port to act as a radiating element while the second port was terminated with a 50Ω load. The result shows convergence the measured and simulated radiation patterns. Minor discrepancies between the measured and simulated patterns can be attributed to limitations in the experimental setup. Figure 11 below shows the highlights that the pattern maintains its shape in the elevation plane across all frequencies. However, at higher frequencies in the azimuth plane, there is a slight alteration in the pattern shape.

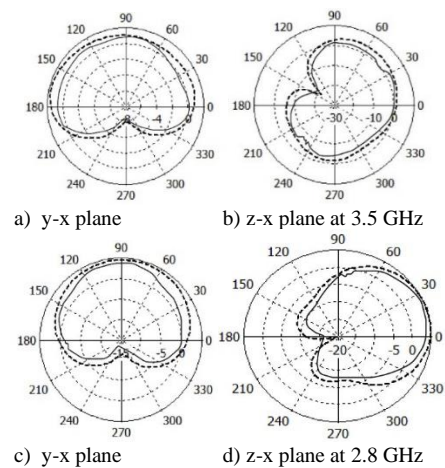


Fig. 11. Simulation (-----) & Measurement (—) results for radiation pattern, “a and c” co-polar and “b and d” cross polar.

C. Envelope Correlation Coefficient

A key metric for assessing the diversity effectiveness of MIMO antennas is the Envelope Correlation Coefficient (ECC). Two primary methods exist for ECC calculation: One is based on the antenna's scattering parameters, while the other is based on the far-field pattern and requires lengthy and complicated computations, offering a relatively simpler approach. For the evaluation of the proposed antenna, the second method, as outlined in [26], is chosen for ECC calculation due to its comparative ease of implementation [28]

$$ECC = \frac{|S_{11}^* S_{12} + S_{21}^* S_{22}|^2}{(1 - |S_{11}|^2 - |S_{21}|^2)(1 - |S_{22}|^2 - |S_{12}|^2)} \quad (6)$$

In an ideal scenario, an uncorrelated MIMO antenna would have an ECC of 0. However, for practical MIMO antennas, a tolerable value is considered to be less than 0.5, as indicated by [27]. The manufactured design exhibits an estimated ECC value of less than 0.01 throughout its whole operating range, as depicted in Figure 12. Additionally, the simulated and measured ECC values closely align. Therefore, the compact MIMO antenna proposed exhibits excellent diversity performance, with minimal correlation between its two antenna ports.

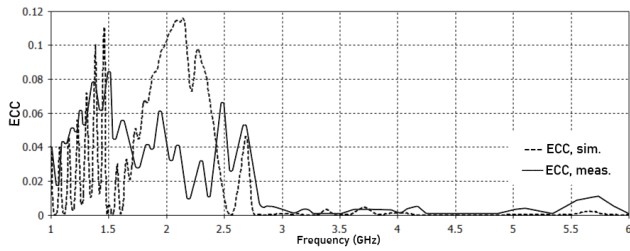


Fig. 12. Envelope correlation coefficient ECC.

D. Diversity Gain & Peak Gain

The diversity gain is another important parameter to evaluate MIMO performance. By using the equation below, can be calculated [28]:

$$DG = 10 \times \sqrt{(1 - ECC^2)} \quad (7)$$

Authors recommended to be close to 10dB for diversity gain to be the effective operation of MIMO antennas [21]. The comparison between the simulated and measured diversity gain of the developed antenna indicates a close match, consistently exceeding 9.9 across the entire frequency range, as shown in Figure 13(a).

Figure 13(b) displays the gain, both simulated and measured for the suggested design. The results reveal a peak gain of 4.6dB at the specified frequency and a gain of 5dB at 2.8 GHz.

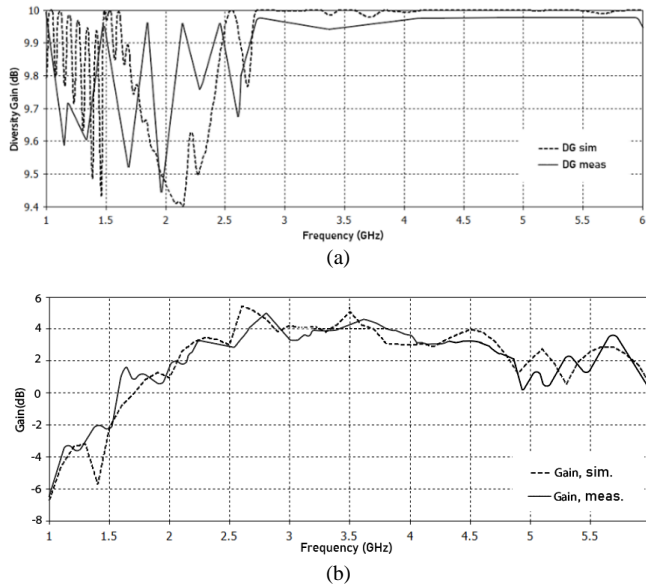


Fig. 13. properties of MIMO design a) Diversity gain, b) Peak gain.

IV. COMPARISON WITH PREVIOUS WORKS

The MIMO antenna design has undergone a comprehensive comparison with recent relevant studies outlined in Table 3, assessing various performance metrics. The evaluation encompasses criteria such as the antenna's channel area (size), operating BW, coupling, desired gain, ECC, diversity gain, and the spatial distance between antenna elements. The findings indicate that our proposed MIMO antenna excels in achieving superior isolation, compact size, and optimal spacing between elements. With these advantages, it emerges as a promising candidate for applications in MIMO systems.

TABLE III
COMPARISON WITH PREVIOUS WORKS

Ref.	Freq. (GHz)	Iso.	ECC	Distance (mm)	Size (mm)	Iso. Tech.
[3]	2.4, 3.5-7.1	-10	0.004	6	32×20×1.8	PE
[4]	2.8-4.3	-20	/	8.8	50×37×1.6	DGS
[5]	2.77-6.55	-15	0.05	10.75	50×25×1.6	DGS with Vias
[6]	1.75-3.00	-22	0.03	-----	40×90×0.8	EBG
[7]	2.8, 4.3, 7.7	-15	0.0001	9.9	64×30×1.6	DGS
[12]	2.38-2.52, 3.28-3.63, 5-6.77	-16	0.005	9	56×30×1.6	NL
This work	2.76-5.32	-20	0.008	7.1	31×50×1.6	MTM & NL

V. CONCLUSION

This study introduces a compact size MIMO antenna, measuring 50mm × 31mm, designed specifically for 5G sub-6 communication. The antenna shows remarkably low mutual coupling, with S₂₁ at 12 < -20dB across the entire operating band and below -28dB at 3.5 GHz. The proposed approach incorporates a t-stub with Moore fractal at the front view and CSRs at the back view. Additionally, CRRs and NL are employed to enhance MIMO performance by minimizing coupling between radiator elements and ensuring impedance matching. After the manufacturing process, the MIMO antenna underwent verification for S-parameters and radiation performance in an anechoic chamber. The measured results closely align with the simulated outcomes, demonstrating excellent MIMO diversity performance. Notably, the antenna achieves a high diversity gain (DG > 9.9) and very low ECC (< 0.008), proving it to be a viable option for 5G sub-6 band MIMO applications.

REFERENCES

- [1] A. Mansoul and M. Nedil, "Compact and Reconfigurable Multiband 2-Element MIMO Slot Antenna for Advanced Communication Systems," 2020 IEEE Int. Symp. Antennas Propag. North Am. Radio Sci. Meet. IEEECONF 2020 - Proc., pp. 575-576, 2020, doi: 10.1109/IEEECONF35879.2020.9330262.
- [2] X. xi Zhang, A. di Ren, and Y. Liu, "Decoupling methods of MIMO antenna arrays for 5G applications: a review," Front. Inf. Technol. Electron. Eng., vol. 21, no. 1, pp. 62-71, 2020, doi: 10.1631/FITEE.1900466.
- [3] S. S. Khade and P. D. Bire, Fractal MIMO antenna for wireless application, vol. 546. Springer Singapore, 2020. doi: 10.1007/978-981-13-6159-3_37.
- [4] L. Ali, M. Ilyas, and T. A. Elwi, "A Metamaterial-Based Compact MIMO Antenna Array Incorporating Hilbert Fractal Design for Enhanced 5G Wireless Communication Networks," Math. Model. Eng. Probl., vol. 10, no. 3, pp. 930-936, 2023, doi: 10.18280/mmep.100324.
- [5] K. V. Prasad and M. V. S. Prasad, "Mutual coupling reduction between slotted-t-mimo elements for uwb applications," Prog. Electromagn. Res. C, vol. 107, no. December 2020, pp. 203-217, 2021, doi: 10.2528/PIERC20091103.
- [6] A. Gupta and V. Kumar, "DGS-based wideband MIMO antenna for on-off body communication with port isolation enhancement operating at 2.45 GHz industrial scientific and medical band," J. Electromagn. Waves Appl., vol. 35, no. 7, pp. 888-901, 2021, doi: 10.1080/09205071.2020.1865209.
- [7] S. R. Pasumathi, J. B. Kamili, and M. P. Avala, "Design of Tri-Band MIMO Antenna with Improved Isolation using DGS and Vias," Wirel.

- Pers. Commun., vol. 110, no. 3, pp. 1523–1532, 2020, doi: 10.1007/s11277-019-06799-9.
- [8] G. Dlvya, K. Jagadeesh Babu, and R. Madhu, “Quad-band hybrid DRA loaded MIMO antenna with DGS for isolation enhancement,” *Int. J. Microw. Wirel. Technol.*, vol. 14, no. 2, pp. 247–256, 2022, doi: 10.1017/S1759078721000519.
- [9] A. M. Ibrahim, I. M. Ibrahim, and N. A. Shairi, “Review isolation techniques of the MIMO antennas for Sub-6,” *Prz. Elektrotechniczny*, vol. 97, no. 1, pp. 3–9, 2021, doi: 10.15199/48.2021.01.01.
- [10] R. Shao, J. Wang, X. Wang, and Y. Wang, “Eight-port Diagonal Antenna with High Isolation and High Efficiency for 5G Smartphone,” *Appl. Comput. Electromagn. Soc. J.*, vol. 37, no. 8, 2023, doi: 10.13052/2022.aces.j.370805.
- [11] M. Mishra, S. Chaudhuri, R. S. Kshetrimayum, and H. Chel, “Low mutual coupling six-port planar antenna for the MIMO applications,” *Int. J. RF Microw. Comput. Eng.*, vol. 30, no. 12, pp. 1–10, 2020, doi: 10.1002/mmce.22439.
- [12] C. Du, Z. Zhao, X. Wang, and F. Yang, “A compact cpw-fed triple-band mimo antenna with neutralization line decoupling for wlan/wimax/5g applications,” *Prog. Electromagn. Res. M*, vol. 103, no. July, pp. 129–140, 2021, doi: 10.2528/PIERM21042301.
- [13] S. Sharma and M. Kumar, “Pentagonal-shaped slot two port MIMO antenna for sub 6 GHz 5G wireless applications,” *Mater. Today Proc.*, vol. 66, no. October 2021, pp. 3438–3445, 2022, doi: 10.1016/j.matpr.2022.06.131.
- [14] S. Chaimool, B. Sangwijit, P. Pukna, and C. Raklua, “A dual-band dual-polarized MIMO antenna for 700 MHz and Sub-6 GHz 5G systems,” 2020 *Int. Symp. Antennas Propagation, ISAP 2020*, pp. 103–104, 2021, doi: 10.23919/ISAP47053.2021.9391244.
- [15] J. Kulkarni, C. Y. D. Sim, A. Chitre, N. Kulkarni, S. Kulkarni, and R. Talware, “Design and Analysis of Compact 2D MIMO Sub-6 GHz 5G Flexible Antenna,” *Proc. IEEE Madras Sect. Int. Conf. 2021, MASCON 2021*, pp. 2–6, 2021, doi: 10.1109/MASCON51689.2021.9563492.
- [16] K. Kavya, V. S. C. S. Murty, K. G. Sujanth Narayan, and J. A. Baskaradas, “Transceiver Design with Hybrid Beamforming for Sub 6 GHz MIMO Communication,” 2021 *Int. Conf. Wirel. Commun. Signal Process. Networking, WiSPNET 2021*, pp. 143–147, 2021, doi: 10.1109/WiSPNET51692.2021.9419435.
- [17] Y. Liu, Z. Yang, P. Chen, J. Xiao, and Q. Ye, “Isolation Enhancement of a Two-Monopole MIMO Antenna Array with Various Parasitic Elements for Sub-6 GHz Applications,” *Micromachines*, vol. 13, no. 12, 2022, doi: 10.3390/mi1312123.
- [18] S. Ahmad et al., “A Compact CPW-Fed Ultra-Wideband Multi-Input-Multi-Output (MIMO) Antenna for Wireless Communication Networks,” *IEEE Access*, vol. 10, pp. 25278–25289, 2022, doi: 10.1109/ACCESS.2022.3155762.
- [19] A. R. Al-Tameemi et al., “A Novel Conformal MIMO Antenna Array based a Cylindrical Configuration for 5G Applications,” *Int. Conf. Electr. Eng. Comput. Sci. Informatics*, vol. 2022-October, no. October, pp. 446–451, 2022, doi: 10.23919/EECSI56542.2022.9946617.
- [20] A. R. Al-Tameemi et al., “Triple band fractal based on T stub waveguide for sub-6 of 5G,” *Int. Conf. Electr. Eng. Comput. Sci. Informatics*, vol. 2022-October, no. October, pp. 424–428, 2022, doi: 10.23919/EECSI56542.2022.9946454.
- [21] J. Banerjee, A. Gorai, and R. Ghatak, “Design and analysis of a compact UWB MIMO antenna incorporating fractal inspired isolation improvement and band rejection structures,” *AEU - Int. J. Electron. Commun.*, vol. 122, p. 153274, 2020, doi: 10.1016/j.aeue.2020.153274.
- [22] R. Keshavarz and N. Shariati, “Low profile metamaterial band-pass filter loaded with 4-turn complementary spiral resonator for WPT applications,” *ICECS 2020 - 27th IEEE Int. Conf. Electron. Circuits Syst. Proc.*, pp. 50–53, 2020, doi: 10.1109/ICECS49266.2020.9294811.
- [23] R. Sanmugasundaram, S. Natarajan, and R. Rajkumar, “A compact mimo antenna with electromagnetic bandgap structure for isolation enhancement,” *Prog. Electromagn. Res. C*, vol. 107, no. December 2020, pp. 233–244, 2021, doi: 10.2528/PIERC20111306.
- [24] A. Eslami, J. Nourinia, C. Ghobadi, and M. Shokri, “Four-element MIMO antenna for X-band applications,” *Int. J. Microw. Wirel. Technol.*, vol. 13, no. 8, pp. 859–866, 2021, doi: 10.1017/S1759078720001440.
- [25] A. Pant, M. Singh, and M. S. Parihar, “A frequency reconfigurable/switchable MIMO antenna for LTE and early 5G applications,” *AEU - Int. J. Electron. Commun.*, vol. 131, no. November 2020, 2021, doi: 10.1016/j.aeue.2021.153638.
- [26] F. Ghawbar, A. S. Jumadi, H. A. Majid, F. A. Saparudin, A. S. A. Ghafar, and B. A. F. Esmail, “Compact self-Isolated MIMO antenna system with

low mutual coupling for 5G mobile applications,” 2020 *IEEE Student Conf. Res. Dev. SCORED 2020*, no. September, pp. 200–205, 2020, doi: 10.1109/SCORED50371.2020.9250998.

- [27] S. Agarwal, U. Rafique, R. Ullah, S. Ullah, S. Khan, and M. Donelli, “Double overt-leaf shaped cpw-fed four port uwb mimo antenna,” *Electron.*, vol. 10, no. 24, pp. 1–16, 2021, doi: 10.3390/electronics10243140.
- [28] A. M. Saleh, T. A. Nagim, R. A. Abd-Alhameed, J. M. Noras, and C. H. See, “Mutual coupling reduction of dual-band uni-planar MIMO system using neutralization line technique,” *Appl. Comput. Electromagn. Soc. J.*, vol. 35, no. 2, pp. 167–175, 2020.
- [29] A. H. Mousa, M. Azlishah, B. I. N. Othman, M. Z. Abidin, and A. M. Ibrahim, “Fractal H-Vicsek MIMO Antenna for 5G Communications,” no. 6, pp. 15–20, 2021, doi: 10.15199/48.2021.06.03.



technology.



Professional in Measurement and Verification (CPMV) as well as Registered Electrical Energy Manager (REEM). His work and



systems, and communication systems. He is currently a Professional Engineer registered with the Board of Engineers Malaysia (BEM).



within the academic and professional communities.

Ahmed Raed Al-tameemi received the Bachelor Degree in Computer techniques engineering from dijlah University, Iraq, in 2011 and Master in Nano electronics from Mordovia national university, Russia in 2018. He is Assistant lecturer with the Department of computer techniques Engineering, Al-Nisour University. In the same time, He is manager of IT department in Al-Nisour university. His work and research interest includes, utility communication technology, electromagnetic

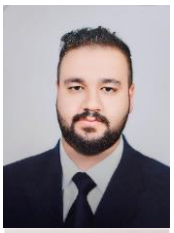
Goh Chin Hock received the Bachelor Degree in Electrical and Electronics Engineering in 2004 as well as Master and PhD in Electrical Engineering in 2008 and 2012 respectively from Universiti Tenaga Nasional, Malaysia. He is currently an Associate Professor with the Department of Electrical and Electronics Engineering, Universiti Tenaga Nasional. He is the Professional Engineer of BEM, Energy Professional of MEPA and Corporate Member of IEM. Besides that, he is Certified Energy Manager (CEM), Certified

Siah Kiong Tiong (Senior Member, IEEE) received the B.Eng. (Hons.), M.Sc., and Ph.D. degrees in electrical, electronics and system engineering from the National University of Malaysia (UKM), in 1997, 2000, and 2006, respectively. He is currently a Professor with the College of Engineering, Universiti Tenaga Nasional, where he is also the Director of the Institute of Sustainable Energy (ISE). His research interests include renewable energy, artificial intelligence, data analytics, microcontroller

Taha Al Sheikhly is a distinguished academic and researcher who earned both his Master's and Ph.D. degrees from Universiti Teknikal Malaysia Melaka (UTeM) in the College of Engineering. With a strong background in engineering and technology, he has contributed to various research areas, particularly in his field of expertise. Currently, he is a faculty member at the University of Technology, Baghdad, Iraq, where he is actively involved in teaching, research, and mentoring students. His work continues to advance engineering knowledge and foster innovation



Mohammed S. Al Ani received the Bachelor Degree in Computer techniques engineering from dijlah University, Iraq, in 2011 and Master in Nano electronics from Mordovia national university, Russia in 2018. Now, a faculty member at Al-Farahidi University with a Master's degree from Russia. My research interests span communications, artificial intelligence (AI), programming, and information systems, with a strong passion for technological advancements and digital transformation. With expertise in modern communication systems and AI-driven applications, I focus on integrating intelligent solutions into various domains, aiming to enhance efficiency and automation. Additionally, my work involves software development and system optimization, ensuring that emerging technologies are effectively applied in both academic and industrial settings.



Mohammed Abdulwahab Khary received the Bachelor Degree in Computer techniques engineering from Baghdad University, Iraq, in 2015 and Master in electronics from Baghdad university, Baghdad, Iraq in 2018. He is Assistant lecturer with the Department of computer techniques Engineering, Al-Nisour University. In the same time. His work and research interest includes, utility communication technology, electromagnetic technology.